



TECHNICAL ARTICLE

Effect of Ultrasonic Impact on Corrosion Fatigue Properties of Titanium Alloy Welded Joints

Xu Yongzhen, Cong Jiahui, Wang Lei, and Hui Li

Submitted: 14 April 2022 / Revised: 18 October 2022 / Accepted: 3 November 2022 / Published online: 17 November 2022

Ultrasonic impact treatment (UIT) is widely used in the aerospace field as a surface treatment technology. The effect of UIT on the corrosion rate and corrosion fatigue properties of TC4 titanium alloy laser welded joints was investigated in this study. On this basis, the surface roughness, surface morphology, microstructure, microhardness and residual stress of samples treated with two different UIT amplitudes (18 and 25 μm) were analyzed. The results showed that compared with the untreated sample, the surface roughness of UIT-treated specimens was increased by 3.9 times but the surface scratches were eliminated. The surface grains of specimens were refined to form a plastically deformed layer $\sim 110 \mu\text{m}$ thick. Compared with the untreated specimens, the hardness of UIT treated specimens were increased by 13.2%, and the hardness influence depth was 0.06 mm. In addition, a high level of compressive residual stress (-529 MPa) was introduced on the surface layer of the specimen. UIT reduced the corrosion rate of the specimen, but the higher UIT amplitude, the worse the reduction effect. UIT treatment improved the corrosion fatigue life of specimens, and the higher UIT amplitude, the more obvious the effect of improvement. The fatigue fracture of the specimens was analyzed by scanning electron microscope. It can be observed that for UIT treated specimens, the fatigue crack source was suppressed inside, the fatigue fringe spacing was reduced, and the dimples were enlarged. Finally, the strengthening mechanism of UIT on the corrosion fatigue properties of the specimens was proposed.

Keywords corrosion fatigue properties, laser welding, ultrasonic impact treatment

1. Introduction

Titanium alloys are among the commonly used engineering materials in many applications ranging from aerospace, transportation, biological applications, and petrochemical industry because of their low density, biocompatibility, weight-to-volume ratio, excellent corrosion resistance, and high strength-to-weight ratio (Ref 1-4). Titanium alloys are characterized by low thermal conductivity, high melting temperature, and high reactivity to oxygen at typical welding temperatures (Ref 5). These inherent material properties of titanium alloys impose stringent demands on welding conditions. The connection technology of titanium alloy develops with the advancement of welding technology. Laser welding is a joining technology of titanium alloys due to its high welding quality,

high welding efficiency, and small welding distortion (Ref 6). However, laser welding of titanium alloys is complicated due to the irregular dispersion of heat, chemical composition, and stress (Ref 7). Additionally, due to the poor thermal conductivity of titanium alloys, the microstructure and mechanical properties of the welds are affected by heat input changes (Ref 8). By optimizing the welding parameters, the static strength of titanium alloy laser-welded joints can be close to that of the raw materials. However, problems still exist with inferior corrosion resistance and fatigue performance (Ref 9). The poor fatigue performance of welded joints is mainly due to the high-value residual tensile stress that causes local stress concentration. The residual tensile stress decreases the corrosion resistance of the welded joint to below that of the base metal (Ref 10, 11). Therefore, the post-weld treatment technology of welded joints has received extensive attention and development. Ultrasonic impact treatment (UIT), as a post-weld treatment technology, is an effective method to improve the corrosion resistance and fatigue performance of materials (Ref 12-13). During UIT, the high-frequency ultrasonic vibration of the impact pin continuously impacts the material, causing plastic deformation on the material's surface, grain size reduction, microstructural refinement, and effectively eliminates residual tensile stress, introduces residual compressive stress, and improves surface hardness, thereby improving the material's corrosion resistance and fatigue performance (Ref 14-15). Lesyk (Ref 16) et al. found that the corrosion potential increased significantly after UIT, the attenuation of the corrosion current, and the protection efficiency (P_{EF}) improvement through the polarization experiments, indicating that the corrosion rate of 1045 steel specimens decreased. P_{EF} of the passive film increased by 21% for the UIT processed surfaces. According to Daavari

Xu Yongzhen, Department of Mechanical and Electrical Engineering, Shenyang Aerospace University, Shenyang 110136, China; **Cong Jiahui**, Department of Mechanical and Electrical Engineering, Shenyang Aerospace University, Shenyang 110136, China; and Key Laboratory of Fundamental Science for National Defense of Aeronautical Digital Manufacturing Process, Shenyang 110136, China; and **Wang Lei** and **Hui Li**, Key Laboratory of Fundamental Science for National Defense of Aeronautical Digital Manufacturing Process, Shenyang 110136, China. Contact e-mail: congjiahui2011@163.com.

et al., UIT positively affected welded pipes under simultaneous fatigue loads and corrosive environments (Ref 10). UIT induces the residual compressive stress of the welded pipe, causing plastic deformation and increased corrosion resistance due to the residual tensile stress reduction. However, relatively few studies exist on the changes in the corrosion resistance and corrosion fatigue performance of welded parts by UIT.

This article describes the effect of UIT on the corrosion resistance and corrosion fatigue properties of TC4 titanium alloy laser-welded joints. This study investigates the changes in corrosion resistance and corrosion fatigue characteristics of welded parts treated by UIT. Experiments to reveal the corrosion mechanism include residual stress evaluation, microhardness test, microstructure analysis, electrochemical corrosion test, surface morphology analysis, and corrosion fatigue, and fracture morphology. Finally, the strengthening mechanism of UIT on the corrosion fatigue properties of the specimens was proposed.

2. Material and Methods

2.1 Materials

The metal used herein is a 2-mm thick TC4 titanium alloy plate. The chemical composition (wt.%) of TC4 titanium alloy is composed of 4.15Al, 6.32 V, 0.3Fe, 0.03C, 0.035 N, 0.065O, 0.0005H and Bal and its tensile strength, yield strength and elongation are 895 MPa, 870 MPa and 10%, respectively. Then, to eliminate the contaminants adhering to the surface of the metal plate, the sheet metals were mechanically polished using sandpapers of grit sizes ranging from 400 to 1000, wiped with absolute ethanol, and dried in a drying flask.

2.2 Laser Welding

The TC4 titanium alloy plates were laser welded using an automatic welding system comprising two parts: a 3000-W all-solid-state laser and a matching welding robot. According to preliminary tests, the optimized laser welding process parameters were selected (Table 1). Before welding, the surfaces of the test panels were mechanically treated using sandpapers of grit sizes ranging from #1200 up to #2000 to remove the surface oxide layer. To prevent welding deformation of the plate, an antideformation fixture was used. Welding was performed in a closed room-temperature environment, and protective gas was used to protect the welded joints from oxygen during the process. The weldments were cut by wire according to the specimen size. The specimens' sizes are shown in Fig. 1.

2.3 Ultrasonic Impact Treatment

The UIT experiment was conducted at room temperature (25 °C). The specimen was mounted on the fixture. During the

Table 1 Laser welding process parameters

Laser welding parameters	Value
Welding power (W)	3000
Welding speed (mm·s ⁻¹)	2
Shielding gas	Argon
Protective gas flow (l·min ⁻¹)	6

impact process, the impulse needle was perpendicular to the weld and was swung at a certain angle perpendicular to the weld direction. A certain amount of pressure was applied to the impact gun to ensure a smooth impact process. The impact degree was characterized by the ultrasonic impact time per unit area (10 × 10 mm²). The selected UIT process parameters are listed in Table 2. The schematic of UIT process is shown in Fig. 1.

2.4 Surface Topography Observation and Roughness Test

The surface morphologies of different treatment forms were observed using an optical microscope. A roughness tester was used to perform three measurements in different areas of the weld area, and the average roughness value of the three measurements was obtained.

2.5 Microstructural Observations

The welded joint was wire-cut and made into a metallographic pattern. The metallographic patterns were mechanically treated using sandpapers of grit sizes ranging from 400 to 3000 to ensure smoothness. The surface of the pattern was etched with an etching solution of 1% HF + 2% HNO₃ + 97% H₂O (vol.%), and finally observed using an optical microscope.

2.6 Residual Stress Test

The residual stresses on the surfaces of the weldments with and without UIT were measured using x-ray diffraction. The working voltage and current were 30.00 kV and 1.20 mA, respectively. The source of the x-ray was Cu K α radiation. Herein, to guarantee the veracity of the experimental data, the measurements were triplicated for each condition to obtain the average value.

2.7 Microhardness Test

A digital hardness tester was employed to measure the microhardness characteristics of the welded joints along the depth directions and surfaces with and without UIT impacts. The loading time and load mass were set to 12 s and 9.8 N, respectively. The indentation method was used to evaluate the microhardness. The measurement surface was smoothed to reduce measurement errors.

2.8 Electrochemical Corrosion Test

Potentiodynamic polarization tests were developed at room temperature using an electrochemical workstation in 3.5 wt.% NaCl solution. The test solution temperature was set constant at 25 °C. The sample was soaked in the solution for 5 min before the test, and the reference electrode (saturated calomel electrode) formed a three-electrode system. Electrochemical corrosion test was performed as per ASTM G5-94 standard. The potential dynamic polarization was tested and plotted at a scanning rate of 10 mV·s⁻¹ from -1 to 6 V.

2.9 Corrosion Fatigue Test and Fatigue Fracture Observation

The MTS testing machine of the multifunctional servo-hydraulic testing system for dynamic testing was used for the corrosion fatigue testing of the samples at room temperature. Corrosion fatigue test was performed as per ASTM E466 standard. The fatigue tests were force-controlled tension-

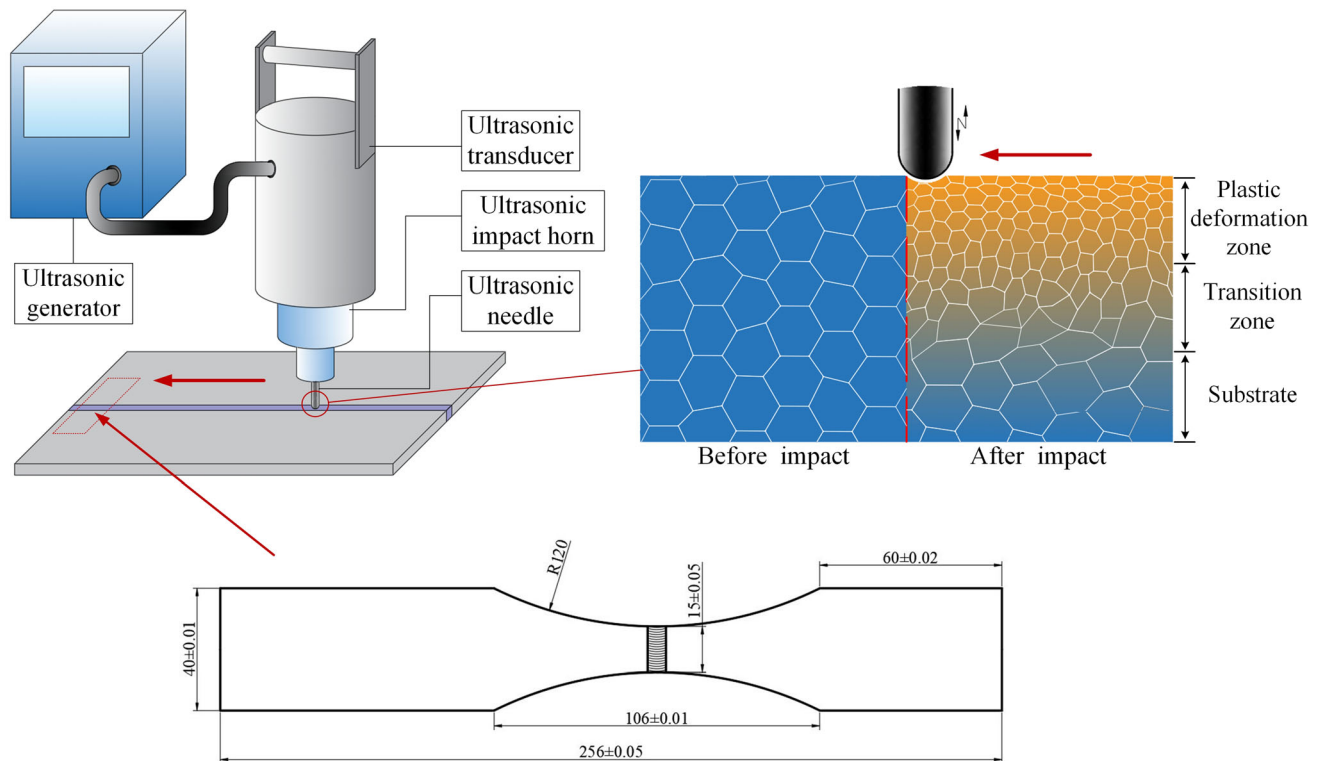


Fig. 1 Schematic of UIT process and specimens' sizes (in mm)

Table 2 UIT parameters used for the sample surface treatment

Ultrasonic impact parameters	Value
Impact amplitude (μm)	18 25
Working current (A)	1.8 2.1
Working frequency (kHz)	17.6
Number of impact needles	1
Impulse needle diameter (mm)	4
Swing speed (mm/min)	130
Processing time (min)	10

tension with a stress ratio (R) = 0.1, and were conducted at 10 Hz. The simulated environment comprised 3.5 wt% NaCl solution. The fatigue fracture was washed with water to remove the corrosive liquid then placed in acetone for ultrasonic cleaning, and finally observed using a scanning electron microscope.

3. Results

3.1 Surface Topography Analysis

The surface morphologies of the specimens before and after UIT at different amplitudes as shown in Fig. 2. Figure 2(a) shows the surface profile of the untreated surface, which is relatively flat overall, but with significant surface damage and poor surface integrity. The surface is marked by interlocking grooves caused by mechanical treatment, which is interlocked, generally in the same direction and of varying depth. Also, the

interlocking and varying thickness of cracks caused by welding on the surface are observed. The surface morphology of UIT at an amplitude of 18 μm , which shows that the surface damage was mitigated, and the surface integrity was improved to some extent (Fig. 2b). The striated gullies become less pronounced, and the fissures taper off. The overall morphology becomes gentle, with some areas of inconspicuous unevenness. The surface morphology after UIT at an amplitude of 25 μm , where the surface damage is significantly less, and the surface flatness is better (Fig. 2c). The surface profile is smooth and free of obvious striations and cracks, but some inner areas are uneven. Hence, UIT effectively improved the surface damage caused by welding and mechanical treatment, resulting in better surface integrity and effectively improving the surface properties of welded joints. However, with increasing amplitude, the uneven deformation in some areas caused uneven surface morphologies of the specimens.

3.2 Roughness Analysis

Figure 3 shows the surface roughness characteristics of specimens at different UIT amplitudes. The average surface roughness of the original specimen was 0.210 μm , with impact amplitudes of 18 and 25 μm , corresponding to an average roughness of 0.582 and 0.836 μm . The surface roughness of the specimens with UIT amplitudes of 18 and 25 μm , respectively, was 2.8 and 3.9 times that of the untreated specimens. Evidently, UIT increases the specimen's surface roughness, and the UIT amplitude increases with the surface roughness. This trend occurs because with the high frequency and vibration of the impacting point on the material's surface, the extrusion and deformation of the material accumulate, forming numerous different shaped depressions, eventually increasing the roughness (Ref 17).

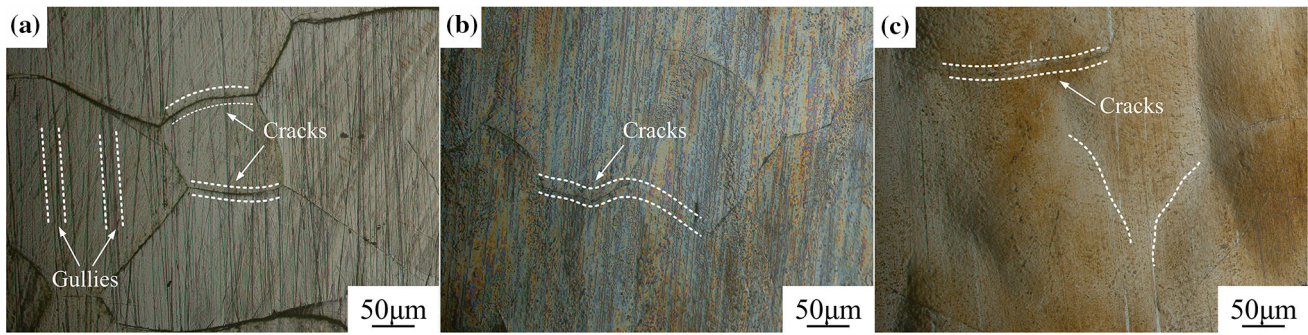


Fig. 2 Surface morphology of UIT treated and untreated specimens: (a) untreated, (b) 18 and (c) 25 μm

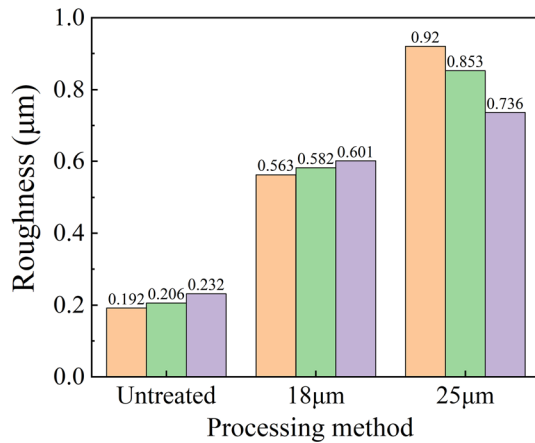


Fig. 3 Surface roughness of UIT treated and untreated specimens: (a) untreated, (b) 18 and (c) 25 μm

3.3 Microstructure Analysis

The microstructures of specimens before and after UIT at different amplitudes are shown in Fig. 4. Evidently, the microstructure without UIT was in the form of equiaxed crystals with uniform size, which was insignificantly different from the matrix structure (Fig. 4a). Figure 4(b) and (c) show the microstructure after UIT. Obviously, the microstructure undergoes plastic deformation, the surface grains are refined, the grain boundaries become blurred, and the color of the deformed layer deepens, which significantly differs from the matrix structure. Grain refinement and increase in grain boundaries deepen the color of the plastically deformed layer (Ref 18). The plastic deformation layer thickness formed after UIT at amplitudes of 18 and 25 μm is ~ 90 and 110 μm , respectively. The plastic deformation layer with ultrasonic impact amplitude of 25 μm is thicker and darker, indicating that UIT with larger amplitude greatly impacted the plastic deformation degree on the material's surface and a deeper impact on the material's interior. In contrast, the grain refinement-strengthening effect caused by UIT keeps the strain inside and outside the grain at the same level, resulting in uniform stress on the welded joint, thereby inhibiting crack initiation (Ref 19). Also, the grain refinement caused by UIT enhances the passivation film formation on the material's surface, thereby improving corrosion resistance (Ref 20). Thus, the grain refinement and plastic deformation induced by UIT improved the corrosion fatigue performance of welded joints and increased the corrosion fatigue life.

3.4 Residual Stress Analysis

Residual tensile stress can impair the fatigue life and corrosion resistance of welded joints (Ref 1, 21). The residual stress distribution on the surface of the specimens before and after UIT at different amplitudes is displayed in Fig. 5. The residual stress in the original specimens is mainly in the form of tensile stresses, with a maximum residual tensile stress of 123 MPa in the weld area and an average value of 116 MPa. The residual tensile stress is unevenly distributed and decreases as the distance from the center of the weld increases. High levels of tensile residual stress and uneven stress distribution in the weld area result from uneven thermal expansion and contraction during welding and cooling (Ref 22). After UIT, the residual stress on the surface of the specimens' changes from residual tensile stress to residual compressive stress. As the distance to the center of the weld increases, the residual compressive stress gradually decreases, and the curve shows an upward trend. The stress distribution tends to be homogeneous, with average residual stresses of -433 and -529 MPa, corresponding to impact amplitudes of 18 and 25 μm . Apparently, the surface residual compressive stress increases with increasing ultrasonic impact amplitude. According to the Goodman formula (Ref 23), the fatigue limit change caused by UIT can be determined as follows: $\Delta\sigma^r = -m\sigma_r$, where $\Delta\sigma^r$ is the material's fatigue limit, m is the average sensitivity coefficient, and σ_r is the residual stress. The material's fatigue limit increases with the participating compressive stress induced by UIT. Thus, the residual compressive stress increases with an increase in ultrasonic impact amplitude before saturation, which increases the fatigue limit and prolongs the fatigue life of specimens.

3.5 Microhardness Analysis

Most cracking originates at the material's surface, and an increase in microhardness can inhibit cracking and improve the material's fatigue properties (Ref 24). The surface microhardness and microhardness with the depth of specimens before and after UIT at different amplitudes as shown in Fig. 6. The average microhardness of the weld zone (WZ) of the original welded joint are 375.4 HV (Fig. 6a). The average microhardness of WZs treated at amplitudes of 18 and 25 μm are 414.8 and 425.1 HV, an increase of 10.5 and 13.2%, respectively, compared to the original WZ. The increase in microhardness caused by UIT was mainly attributable to grain hardening and work hardening effects (Ref 25). As the distance from the surface increases, the microhardness values of the original welds fluctuate in a small range, between 360 and 370 HV, with

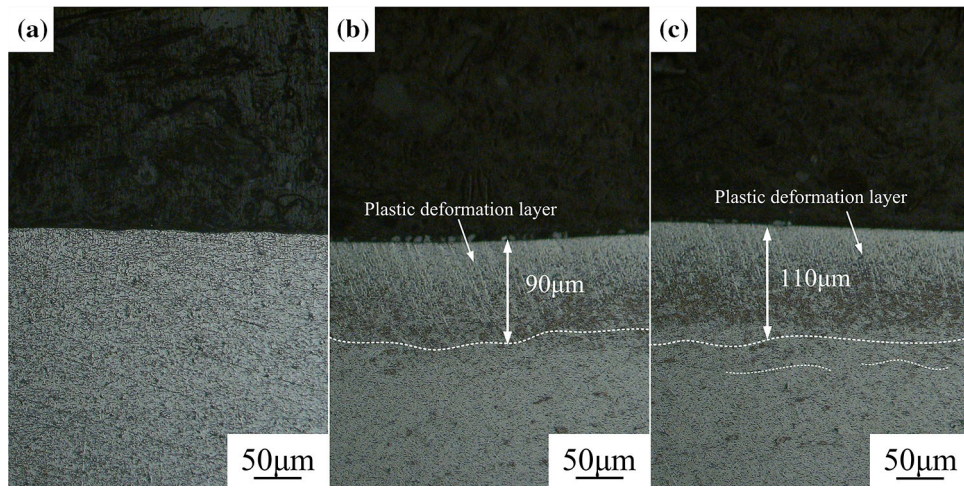


Fig. 4 Microstructures of UIT treated and untreated specimens: (a) untreated, (b) 18 μm , and (c) 25 μm

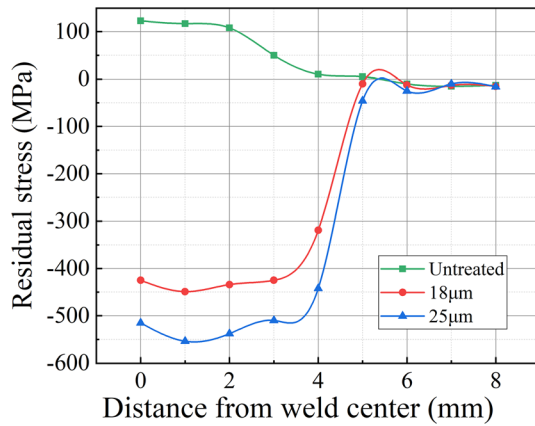


Fig. 5 Residual stress of UIT treated and untreated specimens

an average value of 364.3 HV (Fig. 6b). The internal hardness value of the weld after UIT increases significantly and decreases with increasing depth from the surface, eventually leveling off. The depths of hardness impacts for amplitudes of 18 and 25 μm are ~ 0.04 and 0.06 mm, respectively. Comparing the surface microhardness characteristics and depths of impacts for different amplitudes reveals that high amplitude ultrasonic impacts produce higher impact force values, resulting in greater plastic deformation of the specimen surface, ultimately leading to a deeper work-hardened layer and high hardness values.

3.6 Electrochemical Corrosion Analysis

Table 3 and Fig. 7 show the potentiodynamic polarization test plots before and after UIT at different amplitudes. The corrosion potential (E_{corr}) and current density (I_{corr}) were calculated using the Tafel extrapolation of the cathodic and anodic branches of the polarization curve, and the corrosion rate (CR) was calculated using Faraday's law (Ref 26): $CR = I_{\text{corr}} K E_w / \rho_m$, where K is the Faraday constant ($3.272 \times 10^{-3} \text{ mm} \cdot \text{g} \cdot \mu\text{A}^{-1} \cdot \text{cm}^{-1} \cdot \text{yr}^{-1}$), I_{corr} is the corrosion current density ($\mu\text{A} \cdot \text{cm}^{-2}$), E_w is the equivalent weight, which

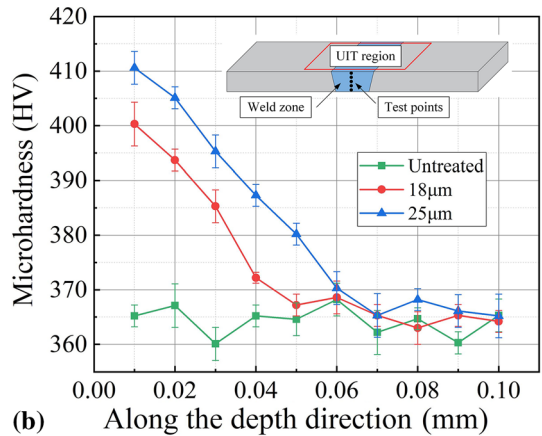
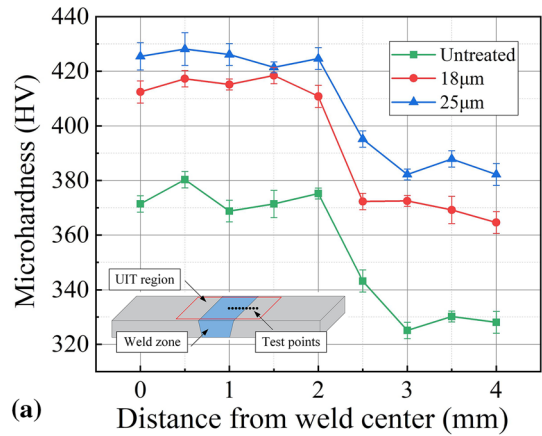


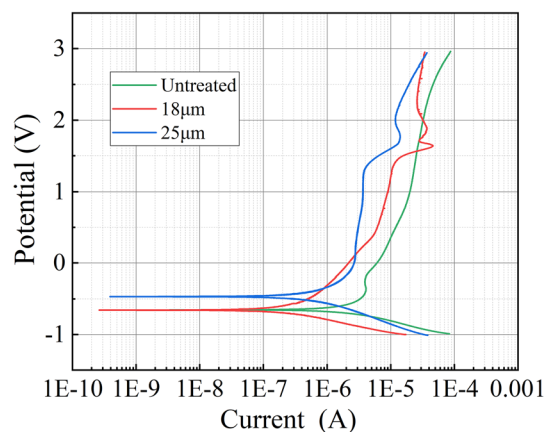
Fig. 6 Microhardness of UIT treated and untreated specimens: (a) surface and (b) micro hardness characteristics at different depths

is 11.98 for Titanium alloy, and ρ_m is the density, the density of titanium alloy is $4.5 \text{ g} \cdot \text{cm}^{-3}$.

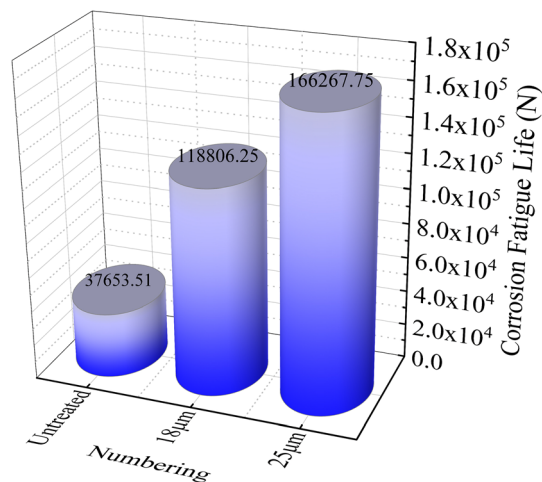
A direct relationship exists between the E_{corr} values and corrosion resistance; the higher the self-corrosion potential, the less susceptible the material is to corrosion (Ref 27). It can be seen from the graph that the corrosion potential of the specimen

Table 3 Electrochemical corrosion characteristics of laser-welded joints of TC4 titanium alloy

Condition	E_{corr} V	I_{corr} , $\mu\text{A}/\text{cm}^2$	Corrosion rate, $\times 10^{-3}$, mm/year
Untreated	- 0.655	1.087	0.947
18 μm	- 0.645	0.175	0.152
25 μm	- 0.426	0.417	0.363

**Fig. 7** Potentiodynamic polarization test plots of UIT treated and untreated specimens

at UIT amplitude of 25 μm exceeds that of the ultrasonic impact-treated specimen at UIT amplitude of 18 μm and the untreated specimen. The untreated and ultrasonic impact-treated specimens at ultrasonic impact amplitudes of 18 and 25 μm exhibit corrosion potentials of - 0.655, - 0.645, and - 0.426 V, respectively. Consequently, the corrosion tendency characteristics of specimens treated at higher amplitudes are lower. The I_{corr} values of the nontreated specimens were 1.087 $\mu\text{A}/\text{cm}^2$, showing a larger active region (Table 3 and Fig. 7). Compared with untreated specimens, the I_{corr} values of specimens with UIT decreased, and secondary passivation occurred during the corrosion process. The I_{corr} values of the ultrasonic impact-treated specimens at amplitudes of 18 and 25 μm are 0.175 and 0.417 $\mu\text{A}/\text{cm}^2$, respectively. The corrosion current density directly reflects the CR, so it can be inferred that UIT effectively reduces the specimen's CR. The enhanced corrosion resistance of samples after UIT was due to the formation of a dense and uniform passive film, which was related to the evolution of the surface microstructure and surface topography (Ref 28). UIT-induced surface grain refinement and residual compressive stress promoted the formation of passivation films and increased the passivation film formation rate, respectively, resulting in improved corrosion resistance (Ref 20). Comparing the I_{corr} values of samples subjected to UIT at different amplitudes shows that the corrosion current density increases with the UIT amplitude. As the UIT amplitude increases, the uniformity and compactness of the passivation film increase while producing higher surface roughness. The higher surface roughness negatively affects the passive film formation and corrosion resistance (Ref 20, 27, 29). Areas with higher surface roughness were the preferred locations for passive film destruction, which increased the CR. Thus, the high-corrosion potential and fast CR of the

**Fig. 8** Corrosion fatigue life of UIT treated and untreated specimens

ultrasonic impact-treated specimen at an amplitude of 25 μm can be inferred.

3.7 Corrosion Fatigue Analysis

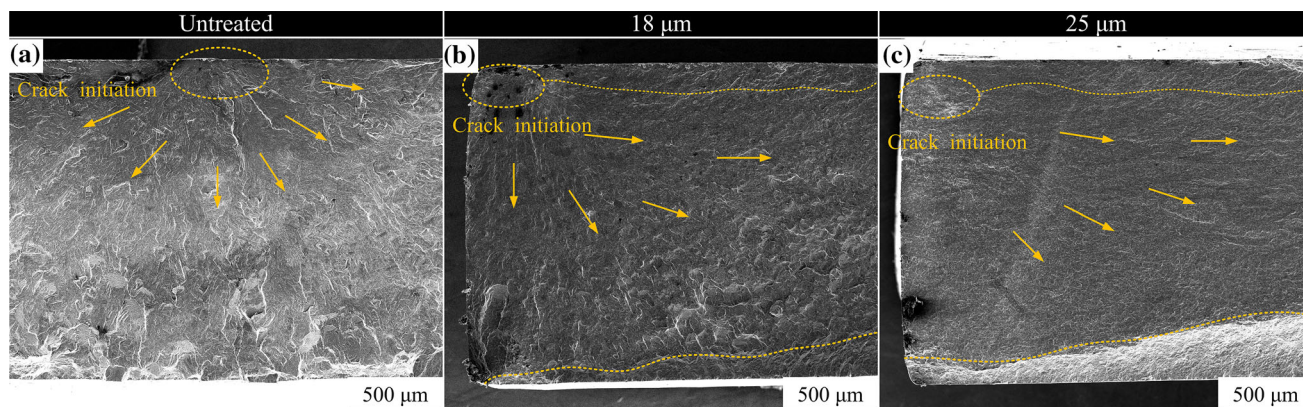
The effects of UIT at different amplitudes on the corrosion fatigue properties of TC4 titanium alloy laser-welded samples as shown in Fig. 8 and Table 4. The corrosion fatigue life of the original specimen is 37653.51 cycles, and the corrosion fatigue lives of UIT-treated specimens at amplitudes of 18 and 25 μm are 118,806.25 and 166,267.75 cycles, respectively, which are 3.16 and 4.42 times that of the original specimen. Obviously, UIT effectively improves the corrosion fatigue life of welded joints, and the corrosion fatigue life of the specimen increases with the UIT amplitude. The fatigue performance effect depends on a combination of extrinsic and intrinsic factors of the specimen (Ref 30). As the amplitude of UIT increases, the improvement in surface damage, the formation of plastic deformation layers, the increase in microhardness, and the introduction of large residual compressive stresses more effectively inhibit crack generation and expansion compared to the negative effect of the increasing surface roughness on the corrosion fatigue performance, thus improving the corrosion fatigue performance.

3.8 Fatigue Fracture Analysis

Figure 9 shows the fatigue fracture morphology before and after UIT at different amplitudes. It can be observed that the source of the cracks in the original specimen originates at the material's surface, and the crack extension area occupies a relatively small portion of the fracture surface (Fig. 9a). The crack propagation extends along the weld thickness, and the propagation route is relatively straight and runs through the

Table 4 Fatigue life statistical parameters

Condition	Number of samples, n	Standard deviation, s	Subsample coefficient of variation, C_v	Median fatigue life, N_{50}
Untreated	4	1553.65	0.04126	37,653.51
18 μm	4	4969.57	0.04183	118,806.25
25 μm	4	6940.96	0.04175	166,267.75

**Fig. 9** Fatigue fracture morphology: (a) untreated, (b) 18 μm , and (c) 25 μm

entire fracture along the weld thickness. From Fig. 9(b), it can be observed that after UIT, the position of fatigue crack initiation is transferred to the material's interior, the fatigue propagation path becomes tortuous, the fatigue propagation direction is deflected to a certain extent, and the crack propagation is significantly hindered near the surface. As shown in Fig. 9(c), the crack source moves further inward, the fatigue extension path becomes more tortuous, the direction of fatigue extension is deflected to a greater extent, and the crack extension is more significantly impeded close to the surface. The ultrasonically impacted weld surface increases the micro-hardness and forms a plastic deformation layer, which effectively inhibits crack initiation and allows cracks to develop in areas of high-stress concentration within the weld. The influence of residual compressive stresses in the reinforcement layer, grain refinement, and plastic deformation layers increases the resistance to the expansion of fatigue cracks to the surface, resulting in a shift in the crack expansion direction and a tortuous crack expansion path, thus extending the crack expansion period.

The fracture morphology of the fatigue crack extension zone is seen in Fig. 10. The entire crack extension path of the untreated specimen is relatively flat and straight, with a single direction and path of crack extension and the presence of some large uncracked surfaces (Fig. 10a). After UIT at an amplitude of 18 μm , the entire crack extension path becomes complex, and the crack extension develops in multiple dimensions and directions (Fig. 10b). Fatigue streaks are unevenly distributed on planes of different heights and orientations, and the crack extension direction changes. As observed in Fig. 10(c), at an ultrasonic impact amplitude of 25 μm , the entire crack extension path becomes more complex, with the direction and dimension of the crack extension constantly changing, shifting

from one plane to another. The increase in grain boundaries caused by grain refinement results in the crack extension direction changes with the different orientations of the grain boundaries, resulting in a tortuous crack extension path (Ref 31). Comparing the magnified areas, A, B, and C (Fig. 10d-f), the fatigue streaks are more widely spaced before UIT. The fatigue stripes become less spaced after UIT, and as the ultrasonic impact amplitude increases, the fatigue stripe spacing decreases further, and secondary cracks are observed. The low spacing of fatigue streaks corresponds to a low crack expansion rate (Ref 32). The residual compressive stress induced by ultrasonic impact has a crack closure effect, which reduces the range of stress intensity factors at the crack tip, thereby reducing the rate of crack expansion (Ref 24). Therefore, it can be deduced that UIT effectively reduces the rate of crack expansion and thus increases the specimen's fatigue life.

From Fig. 11, it can be seen that the fracture morphologies of the transient fracture areas of the samples before and after UIT at different amplitudes. The fracture morphologies of all transient fracture zones show a ductile fracture mode with many dimples. However, the dimples after UIT were larger and deeper, and the size and depth of the dimples further increase with the increase in ultrasonic impact amplitude. In the original sample, the fracture morphology of the transient fracture region mainly comprises small and shallow dimples (Fig. 11a). Compared with dimples of the original specimen, the dimple size and depth of the dimple at UIT amplitude of 18 μm increases (Fig. 11b). When the UIT amplitude increases to 25 μm , the corresponding dimple size and depth further increases. The larger and deeper dimple corresponds to the increase in the willfulness of the material to fracture (Ref 33). Therefore, UIT improves the fracture randomness of TC4 titanium alloy laser-welded joints.

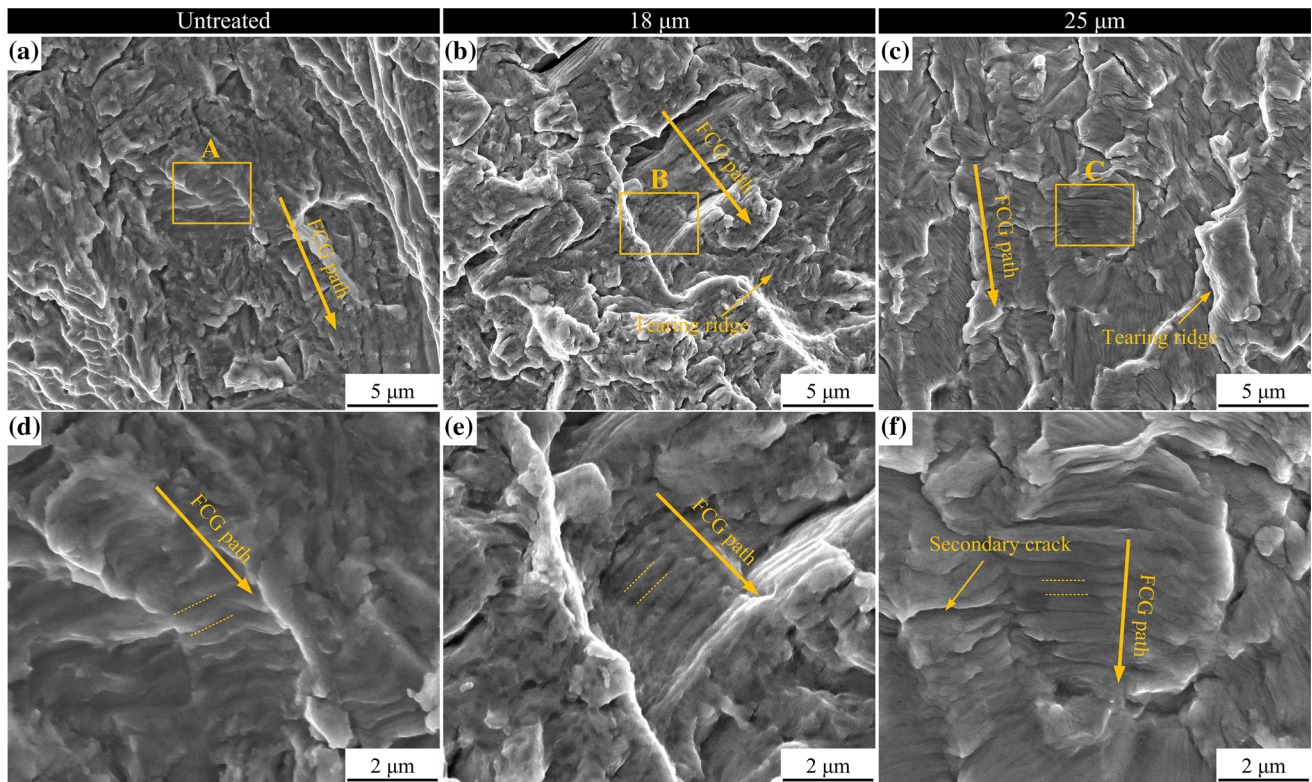


Fig. 10 Fatigue crack extension zone: (a) untreated, (b) 18 μm , (c) 25 μm , and zoom in on areas (d) A, (e) B, and (f) C

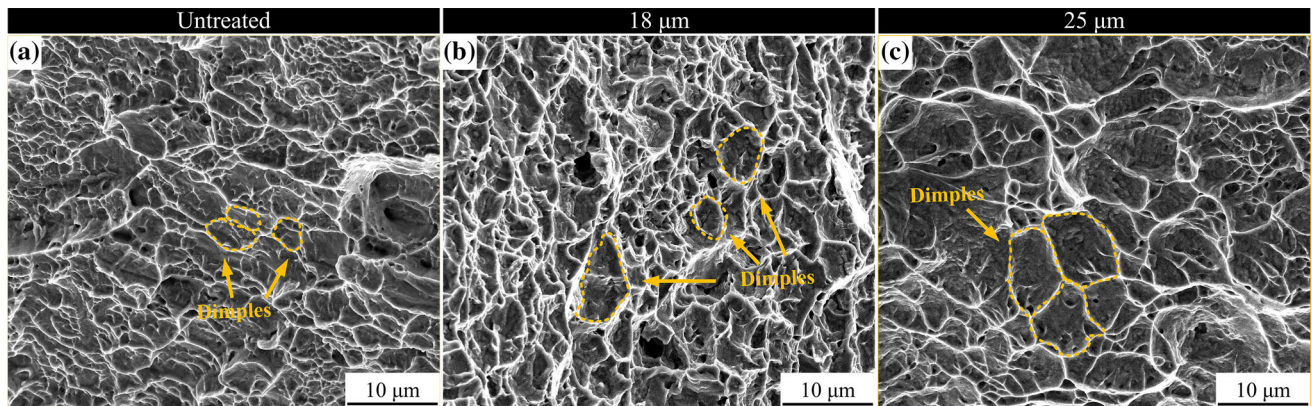


Fig. 11 Transient fracture zone: (a) untreated, (b) 18 μm , and (c) 25 μm

4. Discussion

Based on the above fatigue fracture analysis, the comprehensive effect of ultrasonic impact at different amplitudes on corrosion fatigue performance was comprehensively analyzed. The fatigue fracture principle before and after UIT at different amplitudes is shown in Fig. 12.

Corrosion fatigue failure is a typical fatigue failure under the coupling action of a cyclic load and a corrosive environment. As shown in Fig. 12(a), during the corrosion fatigue process, the transition radius of cracks and scratches caused by welding and mechanical treatment on the surface of laser-welded joints of titanium alloys without UIT is small, which is prone to stress concentration. With the continuous application of an alternating load, high boundary energy is accumulated on the surface of the

welded joint where the stress is concentrated, causing slip deformation on the surface of titanium alloy laser welded joints, where chemically active titanium is exposed to react with the corrosive medium electrochemically (Ref 34). The occurrence of fatigue pitting intensifies the local stress concentration continuously, resulting in faster initiation of crack sources on the welded joint surface. During crack propagation, the residual tensile stress generated by welding is superimposed on the external load stress, increasing the actual load stress. Also, the alternating stress destroys the integrity of the passivation film and accelerates the crack propagation rate until the specimen breaks.

As shown in Fig. 12(b), after the 18 μm UIT, the surface quality of the titanium alloy laser welded joint is improved, the transition radius of the surface groove marks is enlarged, and

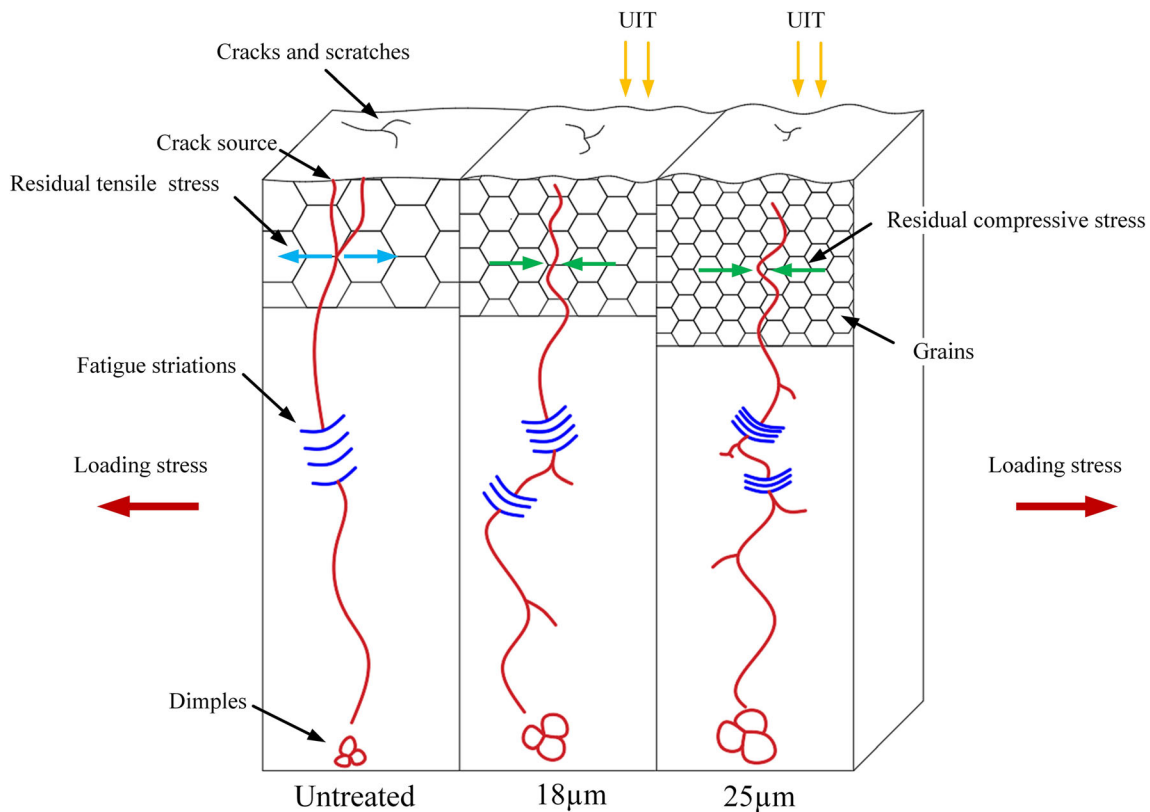


Fig. 12 Fatigue fracture principle of UIT treated and untreated specimens

the degree of stress concentration is reduced. The grain refinement on the welded joint surface caused by ultrasonic impact increases the surface hardness and densifies the structure, forms a plastic deformation layer, inhibits the generation of cracks on the surface, and finally moves the crack source to the material's interior. During the corrosion fatigue process, the grain-refined plastic deformation layer effectively enhances the material's ability on the surface of the titanium alloy laser welded joint to resist slip deformation, hinders the rupture of the passivation film, and thus enhances the laser welded joint's corrosion resistance. Also, more grain boundaries of the surface layer of the welded joint are caused by grain refinement, which blocks crack propagation, making the crack propagation path more tortuous and prolonging the crack propagation. UIT removes residual tensile stress and introduces residual compressive stress in laser welded joints of titanium alloys. The residual compressive stress balances the externally applied load of the corrosion fatigue test and effectively delays the rupture of the passivation film on the surface of the welded joint. However, the crack tip produces a closing effect under residual compressive stresses, which reduces the range of stress intensity factors at the crack tip, thereby reducing the corrosion fatigue crack growth rate and improving the corrosion fatigue resistance of the welded joint. As shown in Fig. 12(c), the degree of grain refinement increases and becomes more uniform as the ultrasonic impact amplitude increases to 25 μm . Also, the residual compressive stresses induced on the surface of the welded joint are increased. Therefore, under the combined effect of residual compressive stress and grain refinement, the corrosion fatigue performance of welded joints is more effectively improved.

Hence, the grain refinement and residual compressive stress induced by ultrasonic impact suppress the CR and the generation of crack sources. Also, the fatigue fringe spacing is shortened, resulting in deeper and larger dimples, effectively slowing the crack growth rate and improving the material toughness.

5. Conclusions

Herein, the effect of UIT on the corrosion fatigue properties of laser-welded joint specimens of TC4 titanium alloy was discussed. Some important conclusions were drawn as follows:

1. The surface roughness of the specimens with UIT amplitudes of 18 and 25 μm , respectively, was 2.8 and 3.9 times that of the untreated specimens. However, surface scratches and cracks were eliminated by UIT.
2. After UIT treatment, the surface microhardness of the specimens with amplitudes of 18 and 25 μm increased by 10.5 and 13.2%, and produced hardness layers of 0.04 and 0.06 mm. In addition, a high level of compressive residual stress was introduced into the surface of the specimen, inducing residual compressive stresses of 433 and -529 MPa at amplitudes of 18 and 25 μm .
3. Compared with the untreated specimens, the corrosion rate of the specimens with amplitudes of 18 and 25 μm was reduced by 83.9 and 61.7%, respectively, and the fatigue life was 3.16 and 4.42 times that of the untreated specimens, respectively.

- After UIT, the position of the crack source moved from the surface to the inside, the crack propagation path became tortuous, and the fatigue band spacing decreased, which was the direct evidence that UIT reduced the crack propagation rate.

Author Contribution

YX: software; conceptualization; validation; validation; formal analysis; data curation; writing—original draft preparation; writing—review and editing; visualization. JC: supervision; project administration; project administration; supervision, funding acquisition. LW: conceptualization; methodology; validation. LH: investigation; resources.

Funding

This research was supported by National Defense Key Laboratory Open Fund of China (SHSYS201901) and State Key Laboratory Open Project of China (VCAME201908) and Project of Education Department of Liaoning Province (JYT2020037).

Conflict of interest

The authors declare no competing interests.

Ethics Approval

We are sure that the manuscript does not violate the ethics approval.

Consent to Participate

All authors agreed to participate.

Consent for Publication

All authors have read and agreed to publish the manuscript.

References

- S.T. Auwal, S. Ramesh, F. Yusof and S.M. Manladan, A Review on Laser Beam Welding of Titanium Alloys[J], *Int. J. Adv. Manuf. Technol.*, 2018, **97**, p 1071–1098
- A. Squillace, U. Prisco, S. Ciliberto and A. Astarita, Effect of Welding Parameters on Morphology and Mechanical Properties of Ti-6Al-4V Laser Beam Welded Butt joints[J], *J. Mater. Process. Technol.*, 2012, **212**, p 427–436
- C. Kumar, C.P. Manas Das and K.S.B. Paul, Comparison of Bead Shape, Microstructure and Mechanical Properties of Fiber Laser Beam Welding of 2 mm Thick Plates of Ti-6Al-4V Alloy [J], *Opt. Laser Technol.*, 2018, **105**, p 306–321
- M. Swapna Sai, V. Dhinakaran, K.P. Manoj Kumar, V. Rajkumar, B. Stalin and T. Sathish, A systematic Review of Effect of Different Welding Process on Mechanical Properties of Grade 5 Titanium Alloy [J], *Mater. Today: Proc.*, 2020, **21**, p 948–953
- F. Fomin and N. Kashaev, Influence of Porosity on the High Cycle Fatigue Behaviour of Laser Beam Welded Ti-6Al-4V Butt Joints [J], *Procedia Struct. Integr.*, 2017, **7**, p 415–422
- X. Gao, L. Zhang, J. Liu and J. Zhang, A Comparative Study of Pulsed Nd: YAG Laser Welding and TIG Welding of Thin Ti6Al4V Titanium Alloy Plate [J], *Mater. Sci. Eng., A*, 2013, **559**, p 14–21
- V. Paranthaman, V. Dhinakaran, M. Swapna Sai and A. Devaraju, A Systematic Review of Fatigue Behavior of Laser Welding Titanium Alloys [J], *Mater. Today: Proc.*, 2021, **39**, p 520–523
- X. Zhan, Q. Peng, Y. Wei and Ou. Wenmin, Experimental and Simulation Study on the Microstructure of TA15 Titanium Alloy Laser Beam Welded Joints [J], *Opt. Laser Technol.*, 2017, **94**, p 279–289
- C. Kumar, C.P. Manas Das and B.S. Paul, Experimental Investigation and Metallographic Characterization of Fiber Laser Beam Welding of Ti-6Al-4V Alloy Using Response Surface Method [J], *Opt. Lasers Eng.*, 2017, **95**, p 52–68
- M. Daavari and S.A. Sadough Vanini, Corrosion Fatigue Enhancement of Welded Steel Pipes by Ultrasonic Impact Treatment [J], *Mater. Lett.*, 2015, **139**, p 462–466
- A. Chattopadhyay, G. Muvvala, S. Sarkara, V. Racherla and A. Kumar Nath, Effect of Laser Shock Peening on Microstructural, Mechanical and Corrosion Properties of Laser Beam Welded Commercially Pure Titanium [J], *Opt. Laser Technol.*, 2021, **133**, p 106527
- M.A. Vasylyev, S.P. Chenakin and L.F. Yatsenko, Ultrasonic Impact Treatment Induced Oxidation of Ti6Al4V Alloy [J], *Acta Mater.*, 2016, **103**, p 761–774
- T. Suzuki, T. Okawa, H. Shimanuki, T. Nose, N. Ohta, H. Suzuki et al., Effect of Ultrasonic Impact Treatment (UIT) on Fatigue Strength of Welded Joints [J], *Adv. Mater. Res.*, 2014, **996**, p 736–742
- M. Malaki and H. Ding, A Review of Ultrasonic Peening Treatment [J], *Mater. Des.*, 2015, **87**, p 1072–1086
- A.I. Dekhtyar, B.N. Mordyuk, D.G. Savvakina, V.I. Bondarchuk, I.V. Moiseeva and N.I. Khripta, Enhanced Fatigue Behavior of Powder Metallurgy Ti-6Al-4V Alloy by Applying Ultrasonic Impact Treatment [J], *Mater. Sci. Eng., A*, 2015, **641**, p 348–359
- D.A. Lesyk, B.N. Mordyuk, S. Martinez, M.O. Iefimov, V.V. Dzhemelinskyi and A. Lamikiz, Influence of Combined Laser Heat Treatment and Ultrasonic Impact Treatment on Microstructure and Corrosion Behavior of AISI 1045 Steel [J], *Surf. Coat. Technol.*, 2020, **401**, p 126275
- A. Panin, A. Dmitriev, A. Nikonov, M. Kazachenok, O. Perevalova and E. Sklyarova, Transformations of the Microstructure and Phase Compositions of Titanium Alloys during Ultrasonic Impact Treatment Part I. Commercially Pure Titanium[J], *Metals*, 2021, **11**, p 562–562
- F. Chen, Y. Yang and N. Li, Effect of Ultrasonic Impact Time on Microstructure and Properties of 7A52 Aluminum Alloy Tandem MIG Welded Joint[J], *Int. J. Adv. Manuf. Technol.*, 2021, **116**, p 2687–2696
- S. Huang, Y. Zhu, W. Guo, P. Peng, H. Qiao, X. Diao et al., Effects of Laser Shock Processing on Fatigue Crack Growth in Ti-17 Titanium Alloy [J], *J. Mater. Eng. Perform.*, 2017, **26**, p 817–821
- L. Xing, R. Dou, M. Huimin, Li. Quande, G. Xiufang and L. Bin, Research Progress of the Effect of Surface Nanocrystallization on the Electrochemical Corrosion of Titanium Alloys[J], *Rare Metal Mater. Eng.*, 2021, **50**(6), p 2245–2253
- X. Song, G. Qian, M. Zhao, W. Zhang, W. Ye and S. Hui, Residual Stress Distribution and Mechanical Properties of TA15/BTi-6431S Titanium Alloy Welding Joints by Ultrasonic Impact Treatment [J], *Mater. Sci. Eng.*, 2018, **381**, p 012164
- X. Feng, X. Pan, W. He, P. Liu, Z. An and L. Zhou, Improving High Cycle Fatigue Performance of Gas Tungsten Arc Welded Ti6Al4V Titanium Alloy by Warm Laser Shock Peening[J], *Int J Fatigue*, 2021, **149**, p 106270
- Y.L. Lee, *Fatigue Testing and Analysis: Theory and Practice[M]*, Lucasta Maardt Press, 2005, p 104–177
- S. Huang, J. Zhao, J. Sheng, X. Meng, E. Agyenim-Boateng, D. Ma et al., Effect of Laser Peening with Different Power Densities on Vibration Fatigue Resistance of Hydrogenated TC4 Titanium Alloy[J], *Int. J. Fatigue*, 2020, **131**, p 105335
- B. He, H. Deng, M. Jiang, K. Wei and Li. Li, Effect of Ultrasonic Impact Treatment on the Ultra High Cycle Fatigue Properties of SMA490BW Steel Welded Joints[J], *Int. J. Adv. Manuf. Technol.*, 2018, **96**, p 1571–1577
- R. Walker, Principles and Prevention of Corrosion[J], *Mater. Des.*, 1993, **14**, p 207
- P. Kumar, G.S. Mahobia, S. Mandal, V. Singh and K. Chattopadhyay, Enhanced Corrosion Resistance of the Surface Modified Ti-13Nb-13Zr Alloy by Ultrasonic Shot Peening[J], *Corros. Sci.*, 2021, **189**, p 109597
- Qi. Zhang, B. Duan, Z. Zhang, J. Wang and C. Si, Effect of Ultrasonic Shot Peening on Microstructure Evolution and Corrosion Resistance of

- Selective Laser Melted Ti-6Al-4V Alloy[J], *J. Market. Res.*, 2021, **11**, p 1090–1099
29. A. Chattopadhyay, G. Muvvala, S. Sarkar, V. Racherla and A. Kumar Nath, Effect of Laser Shock Peening on Microstructural, Mechanical and Corrosion Properties of Laser Beam Welded Commercially Pure Titanium [J], *Opt. Laser Technol.*, 2021, **133**, p 106527
 30. Z. Yaoux, J. Weiju, Z. Hengzhang, M. Xiaonan, F. Jianfeng and Z. Lian, Effect of Laser Shock Processing on Residual Stress and Microstructure of Ti834 Titanium Alloy[J], *Rare Metal Mater. Eng.*, 2019, **48**, p 3535–3540
 31. A. Panin, A. Dmitriev, A. Nikonov, M. Kazachenok, O. Perevalova and E. Sklyarova, Transformations of the Microstructure and Phase Compositions of Titanium Alloys during Ultrasonic Impact Treatment. Part I. Commercially Pure Titanium [J], *Metals*, 2021, **11**, p 562
 32. X. Feng, X. Pan, W. He, P. Liu, Z. An and L. Zhou, Improving High Cycle Fatigue Performance of Gas Tungsten Arc Welded Ti6Al4V Titanium Alloy by Warm Laser Shock Peening[J], *Int. J. Fatigue*, 2021, **149**, p 106270
 33. S. Huang, J. Sheng, J.Z. Zhou, X.K. Meng, S.Q. Xu and H.F. Zhang, On the Influence of Laser Peening with Different Coverage Areas on Fatigue Response and Fracture Behavior of Ti-6Al-4V Alloy[J], *Eng. Fract. Mech.*, 2015, **147**, p 72–82
 34. H. Li, Z. Yongsheng, Z. Song, An. Jinlan and W. Lei, Analysis of Corrosion Fatigue Properties of Notched TC21 Titanium Alloy[J], *Rare Metal Mater. Eng.*, 2020, **49**(08), p 2706–2711

Publisher's Note Springer Nature remains neutral with regard to jurisdictional claims in published maps and institutional affiliations.

Springer Nature or its licensor (e.g. a society or other partner) holds exclusive rights to this article under a publishing agreement with the author(s) or other rightsholder(s); author self-archiving of the accepted manuscript version of this article is solely governed by the terms of such publishing agreement and applicable law.